Catalysis Today 146 (2009) 57–62

Contents lists available at ScienceDirect

Catalysis Today

journal homepage: www.elsevier.com/locate/cattod

Hydrogen production by auto-thermal reforming of ethanol over Ni catalyst supported on ZrO_2 prepared by a sol–gel method: Effect of H_2O/P123 mass ratio in the preparation of ZrO_2

Min Hye Youn [a], Jeong Gil Seo [a], Ji Chul Jung [a], Sunyoung Park [a], Dong Ryul Park [a], Sang-Bong Lee [b], In Kyu Song [a,*]

[a] School of Chemical and Biological Engineering, Institute of Chemical Processes, Seoul National University, Shinlim-dong, Kwanak-ku, Seoul 151-744, South Korea
[b] Korea Research Institute of Chemical Technology, Daejeon 305-600, South Korea

ARTICLE INFO

Article history:
Available online 9 December 2008

Keywords:
Hydrogen
Auto-thermal reforming
Ethanol
Zirconia
Nickel catalyst

ABSTRACT

Zirconia (X-ZrO_2) supports were prepared by a sol–gel method using P123 as a crystal structure and physical property controlling agent with a variation of H_2O/P123 mass ratio (X). 20 wt.% Ni catalysts supported on X-ZrO_2 (X = 2, 3, 4, and 5) were then prepared by an incipient wetness impregnation method for use in hydrogen production by auto-thermal reforming of ethanol. The effect of H_2O/P123 mass ratio (X) on the catalytic performance of Ni/X-ZrO_2 (X = 2, 3, 4, and 5) catalysts was investigated. Crystal structure and physical property of zirconia could be controlled by changing the H_2O/P123 mass ratio during the preparation step. All the Ni/X-ZrO_2 (X = 2, 3, 4, and 5) catalysts exhibited complete conversion of ethanol at 500 °C, while product distributions over Ni/X-ZrO_2 (X = 2, 3, 4, and 5) catalysts were different depending on the H_2O/P123 mass ratio. Hydrogen selectivity over Ni/X-ZrO_2 (X = 2, 3, 4, and 5) catalysts was monotonically increased with increasing reducibility of the catalyst and with increasing H_2O/P123 mass ratio. Among the catalysts tested, Ni/5-ZrO_2 with pure tetragonal phase of zirconia showed the best catalytic performance in hydrogen production by auto-thermal reforming of ethanol. High surface area and small nickel crystalline size of Ni/5-ZrO_2 were also responsible for high catalytic performance of Ni/5-ZrO_2 catalyst.

1. Introduction

Hydrogen is considered to be the most viable energy carrier in future due to its clean, renewable, and non-polluting nature [1–3]. Technological advances in hydrogen utilization like fuel cells make hydrogen more important as a next generation fuel [4,5]. Various hydrocarbon sources such as natural gas [6,7], gasoline [8], alcohols [9,10], and biomass [11] have been used for hydrogen production through catalytic reforming processes. In particular, ethanol has served as a promising source for hydrogen production, because it can be easily handled and is widely distributed around the world. In addition, ethanol has attracted much attention as an alternate hydrogen source due to its low toxicity and high volumetric energy density [12–14].

In hydrogen production by auto-thermal reforming of ethanol, nickel-based catalysts have been widely investigated due to their excellent C–C bond cleavage ability and low cost [15]. In general, the identity of support strongly affects the catalytic performance of supported nickel catalysts in the reforming reactions. Among various supporting materials, ZrO_2 is known to be very effective in inhibiting nickel sintering in the presence of water at high reaction temperature [16]. Zirconia also has high thermal stability and strong resistance against coke formation [17]. All these make zirconia well suited as a supporting material for nickel catalysts in the reforming reactions. It was previously reported that nickel catalyst supported on ZrO_2 showed better catalytic performance than that supported on ZnO, MgO, TiO_2, and Al_2O_3 in hydrogen production by auto-thermal reforming of ethanol, due to the favorable modification of electronic structure of nickel species on ZrO_2 [18].

In this work, zirconia (X-ZrO_2) supports were prepared by a sol–gel method using P123 as a crystal structure and physical property controlling agent with a variation of H_2O/P123 mass ratio (X). 20 wt.% Ni catalysts supported on X-ZrO_2 (X = 2, 3, 4, and 5) were then prepared by an incipient wetness impregnation method for use in hydrogen production by auto-thermal reforming of ethanol. The effect of H_2O/P123 mass ratio (X) on the catalytic property and catalytic performance of Ni/X-ZrO_2 (X = 2, 3, 4, and 5) catalysts was investigated.

* Corresponding author. Tel.: +82 2 880 9227; fax: +82 2 889 7415.
E-mail address: inksong@snu.ac.kr (I.K. Song).

0920-5861/$ – see front matter © 2008 Elsevier B.V. All rights reserved.
doi:10.1016/j.cattod.2008.10.028

2. Experimental

2.1. Preparation of ZrO_2 supports and supported Ni catalysts

A series of *X*-ZrO_2 (*X* = 2, 3, 4, and 5) supports were prepared using P123 as a crystal structure and physical property controlling agent with a variation of H_2O/P123 mass ratio (*X*). A solution comprising 10 g of P123 ((ethylene oxide)$_{20}$(propylene oxide)$_{70}$(ethylene oxide)$_{20}$, BASF), 200 ml of 2-butanol, 3 ml of hydrochloric acid (35% HCl, Samchun Chem.), and known amount of water was prepared at 80 °C with constant stirring (Solution A). Another solution composed of 24 ml of zirconium butoxide ($Zr(OBu)_4$, Sigma–Aldrich), 16 ml of diethylene glycol ($C_4H_{10}O_3$, Sigma–Aldrich), and 100 ml of 2-butanol was prepared at room temperature with constant stirring (Solution B). After adding Solution B to Solution A, the resulting solution was stirred for 3 h to obtain a transparent zirconia sol with an aim of forming a different micelle structure of zirconia. The resulting sol was maintained at 100 °C for 24 h in a closed container to form a gel. The obtained product was washed and filtered with ethanol, and then it was dried at 80 °C in a convection oven to obtain a solid. The solid product was finally calcined at 500 °C for 5 h to yield a zirconia support. Zirconia supports prepared with a variation H_2O/P123 mass ratio (*X*) were denoted as *X*-ZrO_2 (*X* = 2, 3, 4, and 5). Ni catalysts supported on *X*-ZrO_2 (*X* = 2, 3, 4, and 5) were prepared by an incipient wetness impregnation method. The supported Ni catalysts were dried at 100 °C for 12 h, and subsequently, they were calcined at 500 °C for 5 h. The prepared catalysts were denoted as Ni/*X*-ZrO_2 (*X* = 2, 3, 4, and 5). Ni loading was fixed at 20 wt.% in all cases.

2.2. Characterization

BET surface areas of supports were obtained with an ASAP-2010 instrument (Micromeritics). Surface morphologies of supports were examined by FE-SEM analyses (Jeol, JSM-6700F). Crystalline phases of supports and supported catalysts were determined by XRD (MAC Science, M18XHF-SRA) measurements using Cu Kα radiation (λ = 1.54056 Å) operated at 50 kV and 100 mA. In order to check the reducibility of supported catalysts, temperature-programmed reduction (TPR) measurements were conducted in a conventional flow system with a moisture trap connected to a thermal conductivity detector at temperatures ranging from room temperature to 1000 °C with a ramping rate of 5 °C/min. For the TPR measurements, a mixed stream of H_2 (2 ml/min) and N_2 (20 ml/min) was used for 0.2 g of catalyst sample.

2.3. Auto-thermal reforming of ethanol

Auto-thermal reforming of ethanol (EtOH) was carried out in a continuous flow fixed-bed reactor at atmospheric pressure. Each calcined catalyst (50 mg) was charged into a tubular quartz reactor, and then it was reduced with a mixed stream of H_2 (10 ml/min) and N_2 (30 ml/min) at 500 °C for 3 h. Ethanol and water were sufficiently vaporized by passing through a pre-heating zone and were continuously fed into the reactor together with N_2 carrier (30 ml/min). Feed ratios of H_2O/EtOH and O_2/EtOH were fixed at 3.0 and 0.5, respectively. Contact time was maintained at 175 g-catalyst min/EtOH-mole. Catalytic reaction was carried out at 500 °C. Ethanol (EtOH) conversion and product selectivity were calculated according to the following equations. Here, *n* represents the number of moles and χ is a stoichiometric factor (χ = 2 for C_1 and χ = 1 for C_2 compounds).

$$\text{EtOH conversion} = \frac{n_{\text{EtOH,in}} - n_{\text{EtOH,out}}}{n_{\text{EtOH,in}}} \times 100 \quad (1)$$

$$\text{H}_2\text{ selectivity} = \frac{n_{\text{H}_2}}{3(n_{\text{EtOH,in}} - n_{\text{EtOH,out}}) + (n_{\text{H}_2\text{O,in}} - n_{\text{H}_2\text{O,out}})} \times 100 \quad (2)$$

$$C_\chi\text{ selectivity} = \frac{n_{C_\chi}}{\chi(n_{\text{EtOH,in}} - n_{\text{EtOH,out}})} \times 100 \quad (3)$$

3. Results and discussion

3.1. Physical property of X-ZrO_2 supports

Fig. 1 shows the FE-SEM images of *X*-ZrO_2 (*X* = 2, 3, 4, and 5) supports calcined at 500 °C. At low H_2O/P123 ratio (*X* = 2 and 3), ZrO_2 retained rod-like surface morphology. With increasing H_2O/

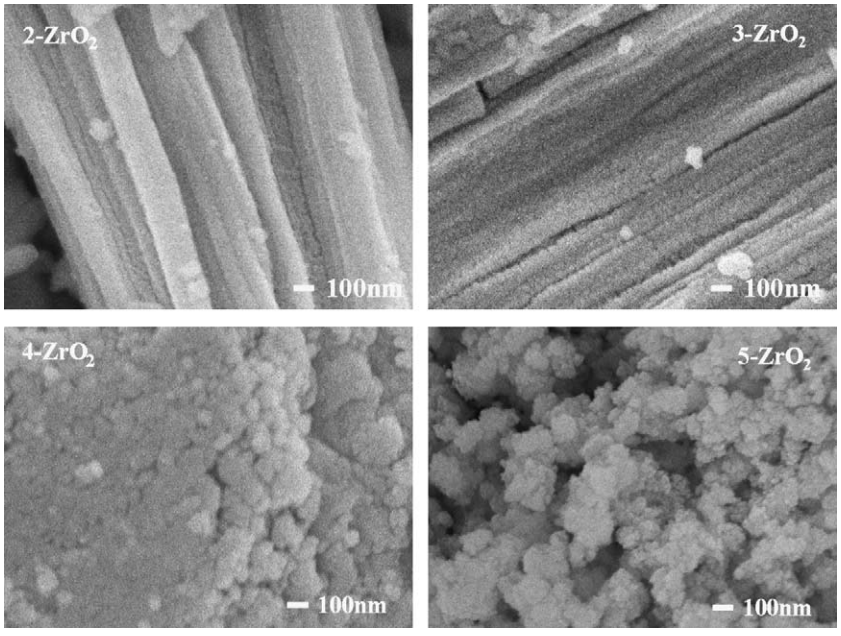

Fig. 1. FE-SEM images of *X*-ZrO_2 (*X* = 2, 3, 4, and 5) supports calcined at 500 °C.

P123 mass ratio (X), however, a drastic change in surface morphology from rod-like shape (X = 2 and 3) to vesicle-like shape (X = 4 and 5) was observed. BET surface areas of X-ZrO_2 (X = 2, 3, 4, and 5) supports increased with increasing H_2O/P123 mass ratio in the order of 2-ZrO_2 (18 m^2/g) < 3-ZrO_2 (27 m^2/g) < 4-ZrO_2 (47 m^2/g) < 5-ZrO_2 (63 m^2/g). The variation of surface area of X-ZrO_2 supports was closely related to the transformation of surface morphology. This was well supported by the previous works [19–21] reporting that concentration of surfactant played an important role in determining the textural and structural properties of sol–gel derived materials. It is known that colloidal behavior and micelle structure of P123 strongly depend on surfactant type, block copolymer composition, solvent nature, and water content in non-aqueous media [22]. Therefore, it is believed that the different micelle shape depending on the H_2O/P123 mass ratio might inevitably affect the surface area and surface morphology of zirconia, as attempted in this work.

3.2. Crystal structure of X-ZrO_2 supports and Ni/X-ZrO_2 catalysts

Fig. 2 shows the XRD patterns of X-ZrO_2 (X = 2, 3, 4, and 5) supports calcined at 500 °C. Each crystalline phase was identified using JCPDS. In the 2-ZrO_2 support, XRD peaks for monoclinic ZrO_2 (JCPDS 00-050-1089) were dominantly observed, although weak peaks corresponding to tetragonal ZrO_2 (JCPDS 27-0997) were also found. With increasing H_2O/P123 mass ratio (X), however, XRD peaks for monoclinic ZrO_2 became weakened and XRD peaks for tetragonal ZrO_2 were gradually developed. And finally, 5-ZrO_2 showed the XRD peaks for pure tetragonal ZrO_2. It can be summarized that monoclinic phase of zirconia was mainly formed in the X-ZrO_2 (X = 2 and 3) supports with rod-like morphology and low surface area, while tetragonal phase of zirconia with vesicle-like morphology and high surface area was dominantly formed at high H_2O/P123 mass ratio (X).

Fig. 3 shows the XRD patterns of Ni/X-ZrO_2 (X = 2, 3, 4, and 5) catalysts calcined and reduced at 500 °C. All the calcined catalysts showed the narrow XRD peaks for NiO, indicating the formation of relatively large NiO particles on the supports (Fig. 3(a)). All the reduced catalysts showed the XRD peaks corresponding to metallic Ni, indicating that NiO was successfully reduced to metallic Ni (Fig. 3(b)). Crystalline sizes of NiO and Ni calculated by the Scherrer equation are listed in Table 1. Crystalline sizes of nickel species were found to be somewhat large. It is believed that the large particle sizes of Ni species were attributed to the relatively large amount (20 wt.%) of Ni loading on the zirconia supports with small surface area. Crystalline sizes of nickel species in the Ni/X-ZrO_2 (X = 2, 3, 4, and 5) catalysts decreased with increasing H_2O/P123 mass ratio (X). Among the catalysts, Ni/5-ZrO_2 showed the smallest crystalline sizes of NiO and Ni.

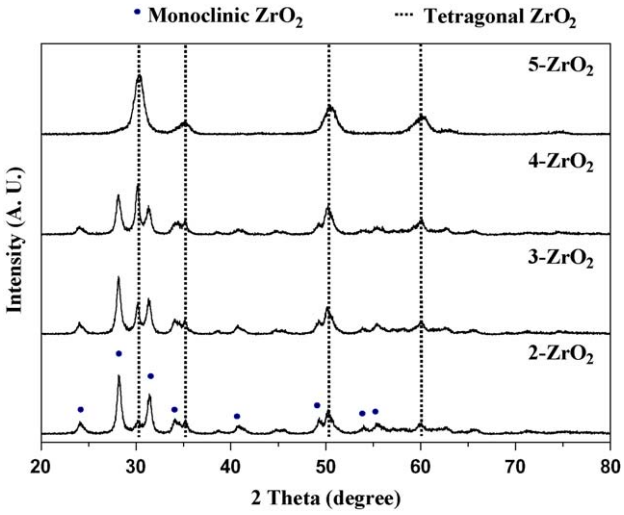

Fig. 2. XRD patterns of X-ZrO_2 (X = 2, 3, 4, and 5) supports calcined at 500 °C.

Table 1
Crystalline sizes of nickel species in the Ni/X-ZrO_2 catalysts.

Catalyst	NiO crystalline size (nm)[a]	Ni crystalline size (nm)[b]
Ni/2-ZrO_2	27.3	31.5
Ni/3-ZrO_2	27.1	28.2
Ni/4-ZrO_2	25.1	27.7
Ni/5-ZrO_2	23.6	24.4

[a] Calculated by the Scherrer equation using (2 0 0) diffraction peak of NiO.
[b] Calculated by the Scherrer equation using (1 1 1) diffraction peak of metallic Ni.

3.3. Reducibility of Ni/X-ZrO_2 catalysts

TPR measurements were carried out to investigate the reducibility of supported nickel catalysts and to see the interaction between nickel and support. TPR measurements were also conducted for X-ZrO_2 supports to investigate the reducibility of supporting materials. However, all the X-ZrO_2 (X = 2, 3, 4, and 5) supports showed no noticeable reduction band. As shown in Fig. 4, reduction profiles of Ni/X-ZrO_2 (X = 2, 3, 4, and 5) catalysts were different depending on the H_2O/P123 mass ratio (X). Ni/X-ZrO_2 (X = 2, 3, and 4) catalysts showed two major reduction peaks

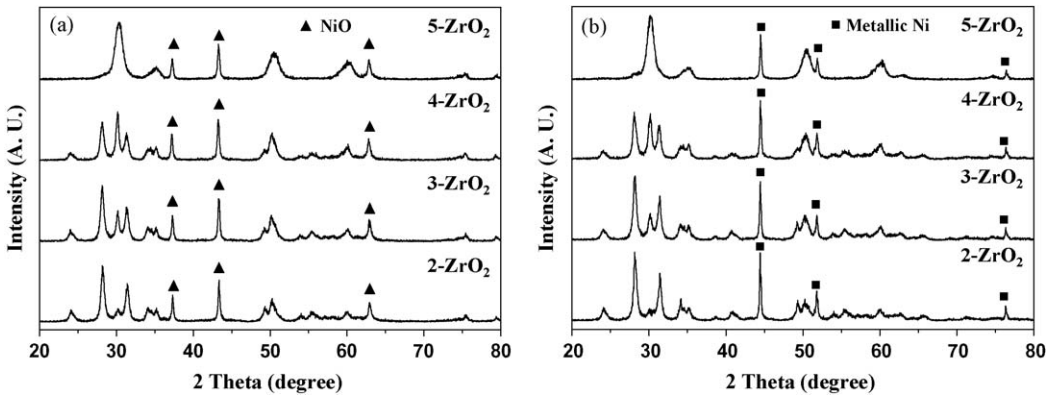

Fig. 3. XRD patterns of Ni/X-ZrO_2 (X = 2, 3, 4, and 5) catalysts (a) calcined and (b) reduced at 500 °C.

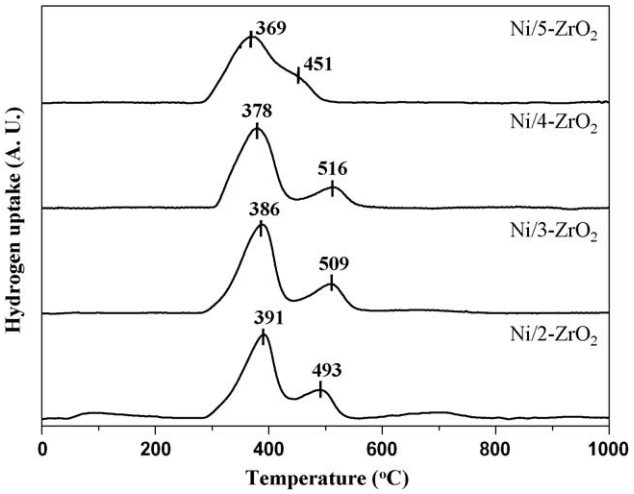

Fig. 4. TPR profiles of Ni/*X*-ZrO_2 (*X* = 2, 3, 4, and 5) catalysts.

within the temperature of 350–550 °C. With increasing H_2O/P123 mass ratio (*X*), the first reduction band appearing at around 380 °C shifted to lower temperature in the Ni/*X*-ZrO_2 (*X* = 2, 3, and 4) catalysts. The reduction peak at around 350 °C is attributed to the reduction of NiO with uniform crystalline size [23]. On the other hand, the second reduction band appearing at around 500 °C shifted to higher temperature and the reduction peak area gradually decreased with increasing H_2O/P123 mass ratio (*X*) in the Ni/*X*-ZrO_2 (*X* = 2, 3, and 4) catalysts. Judging from the fact that monoclinic phase of zirconia became weakened with increasing H_2O/P123 mass ratio (*X*) (Fig. 2), it can be inferred that the second reduction band of Ni/*X*-ZrO_2 (*X* = 2, 3, and 4) catalysts is closely related to the monoclinic phase of zirconia. This means that the first reduction band is closely associated with the tetragonal phase of zirconia. In other words, the low-temperature reduction band may dominantly affect the catalytic performance. Unlike Ni/*X*-ZrO_2 (*X* = 2, 3, and 4) catalysts, Ni/5-ZrO_2 showed one broad reduction peak with a shoulder at around 370 °C. It is known that the reduction peak of bulk NiO species appeared at around of 350 °C [23]. Therefore, it is believed that this reduction behavior of Ni/5-ZrO_2 is closely associated with the reduction of NiO species weakly interacted with tetragonal phase of zirconia. Once again, this result strongly support that the low-temperature reduction band dominantly affects the catalytic performance. The major reduction peak temperature of Ni/*X*-ZrO_2 catalysts decreased in the order of Ni/2-ZrO_2 (391 °C) > Ni/3-ZrO_2 (386 °C) > Ni/4-ZrO_2 (378 °C) > Ni/5-ZrO_2 (369 °C). This result was well supported by the previous work [24] reporting that reduction band of NiO species interacted with monoclinic phase of zirconia appeared at higher temperature than that interacted with tetragonal phase of zirconia. As mentioned earlier (Fig. 2), the addition of large amount of water was favorable for the formation of tetragonal phase of zirconia in our catalyst system, which eventually led to the decreased interaction between nickel species and zirconia. Among the catalysts, Ni/5-ZrO_2 showed the lowest reduction peak temperature. It is interesting to note that the reducibility of Ni/*X*-ZrO_2 catalysts increased with increasing BET surface area of *X*-ZrO_2 supports.

In order to check the degree of reduction, additional TPR measurements were conducted at temperatures ranging from room temperature to 1000 °C. Prior to TPR measurements, the previously reduced Ni/*X*-ZrO_2 catalysts were passivated using O_2 diluted with N_2. The reduction condition was identical to that of the experimental section. It was found that all the catalysts showed no reduction band within the range of room temperature–1000 °C. This result means that all the Ni/*X*-ZrO_2 catalysts were fully reduced in the reduction process employed in this work.

3.4. Catalytic performance of Ni/X-ZrO_2 in the auto-thermal reforming of ethanol

In the auto-thermal reforming of ethanol performed at 500 °C, all the Ni/*X*-ZrO_2 (*X* = 2, 3, 4, and 5) catalysts exhibited complete conversion of ethanol and oxygen. However, product distributions over the catalysts were different depending on the H_2O/P123 mass ratio (*X*). It has been reported that ethanol conversion in the reforming reactions over supported nickel catalysts reaches 100% at temperatures above 500 °C, regardless of space velocity [25–27]. This means that hydrogen selectivity is identical to hydrogen yield under the condition of 100% ethanol conversion. Therefore, the catalytic performance was evaluated in terms of hydrogen selectivity (hydrogen yield) in this work.

Fig. 5 shows the hydrogen selectivity with time on stream in the auto-thermal reforming of ethanol over Ni/*X*-ZrO_2 (*X* = 2, 3, 4, and 5) catalysts at 500 °C. All the catalysts exhibited a stable catalytic performance during the reaction extending over 15 h. The catalytic performance of Ni/*X*-ZrO_2 (*X* = 2, 3, 4, and 5) catalysts increased with increasing H_2O/P123 mass ratio (*X*). Among the catalysts tested, Ni/5-ZrO_2 with pure tetragonal phase of zirconia showed the best catalytic performance in hydrogen production by auto-thermal reforming of ethanol. The hydrogen selectivity over Ni/5-ZrO_2 (52.1%) was higher than that over Ni catalyst supported on commercial ZrO_2 (50.1%) [18]. The enhanced catalytic performance of Ni/5-ZrO_2 was due to the formation of pure tetragonal phase of zirconia, leading to the facile reduction of nickel species. It was reported that pure tetragonal phase of zirconia played an important role in the adsorption of steam and the subsequent spillover of steam from the support to the active nickel [28–30]. This strongly supports our experimental result that Ni/5-ZrO_2 with pure tetragonal phase of zirconia showed the best catalytic performance in the auto-thermal reforming of ethanol.

Fig. 6 shows the correlation between hydrogen selectivity over Ni/*X*-ZrO_2 (*X* = 2, 3, 4, and 5) catalysts and reduction peak temperature of Ni/*X*-ZrO_2 (*X* = 2, 3, 4, and 5) catalysts. The first reduction peak temperature shown in Fig. 4 was taken for the correlation, because the low-temperature reduction band dominantly affects the catalytic performance. It should be noted that hydrogen selectivity over Ni/*X*-ZrO_2 (*X* = 2, 3, 4, and 5) catalysts was monotonically increased with increasing reducibility (with

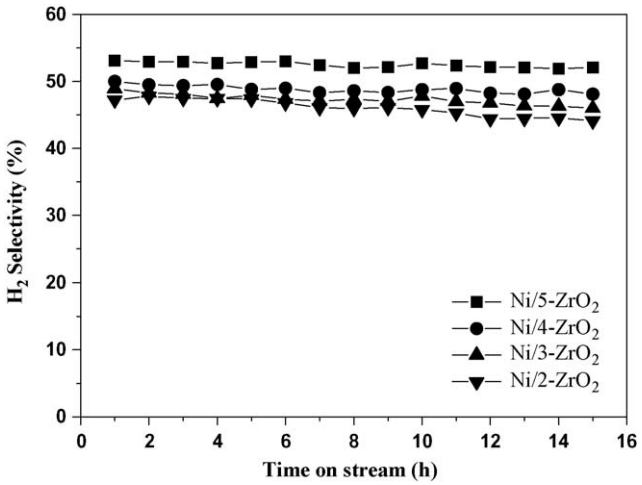

Fig. 5. Hydrogen selectivity with time on stream in the auto-thermal reforming of ethanol over Ni/*X*-ZrO_2 (*X* = 2, 3, 4, and 5) catalysts at 500 °C.

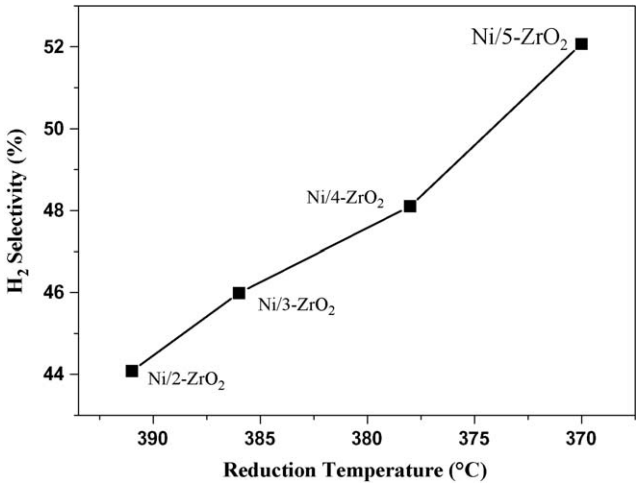

Fig. 6. A correlation between hydrogen selectivity over Ni/*X*-ZrO_2 (*X* = 2, 3, 4, and 5) catalysts and reduction peak temperature of Ni/*X*-ZrO_2 (*X* = 2, 3, 4, and 5) catalysts. Reaction data were obtained after a 15-h reaction.

decreasing reduction peak temperature) and with increasing H_2O/P123 mass ratio (*X*). It is known that interaction between metal and support increases with decreasing metal particle size, leading to the decreased reducibility. Nonetheless, it was observed in our catalyst system that interaction between nickel species and zirconia decreased (reducibility of Ni/*X*-ZrO_2 increased) (Fig. 4) with decreasing crystalline size of nickel species (Table 1). Therefore, it is believed that crystal structure of zirconia rather than crystalline size of nickel species was more closely related to the reducibility of Ni/*X*-ZrO_2 in our catalyst system. Judging from the fact that small crystalline size of metal catalyst is favorable for the catalytic reactions, it can be inferred that small nickel crystalline size of Ni/5-ZrO_2 also served in a positive manner for enhancing the catalytic performance of Ni/5-ZrO_2.

3.5. By-product distribution

To elucidate the effect of H_2O/P123 mass ratio (*X*) on the by-product distribution over Ni/*X*-ZrO_2 (*X* = 2, 3, 4, and 5) catalysts, selectivities for CO, CO_2, CH_4, C_2H_4, and CH_3CHO were measured as listed in Table 2. Selectivities for major carbon products (CO, CO_2, CH_4, C_2H_4, and CH_3CHO) were calculated according to Eq. (3). Carbon balance calculated by the equation of [(carbon number of major carbon products (CO + CO_2 + CH_4 + C_2H_4 + CH_3CHO) formed/carbon number of ethanol converted) × 100] was in range of 82–93%. This means that 7–18% of total carbon was transformed into other carbon species. When considering the formation of extremely small amount of by-products such as acetone, butanal, ethyl acetate, methyl ethyl ketone, and diethoxyethane, it can be inferred that carbon content deposited on the used catalysts was less than 7–18 carbon%.

Table 2
Product distributions over Ni/*X*-ZrO_2 (*X* = 2, 3, 4, and 5) catalysts in the auto-thermal reforming of ethanol at 500 °C.

Catalyst	Selectivity (%)[a]				
	CO	CO_2	CH_4	C_2H_4	CH_3CHO
Ni/2-ZrO_2	9.0	19.9	52.1	4.7	7.6
Ni/3-ZrO_2	8.2	21.3	49.4	2.5	3.1
Ni/4-ZrO_2	7.6	23.9	47.0	1.8	1.8
Ni/5-ZrO_2	6.1	28.4	45.1	0.9	1.7

[a] Product selectivity was obtained after a 15-h reaction.

Selectivity for CO_2 over Ni/*X*-ZrO_2 (*X* = 2, 3, 4, and 5) catalysts increased with increasing H_2O/P123 mass ratio (*X*). On the other hand, selectivities for CO, CH_4, C_2H_4, and CH_3CHO over Ni/*X*-ZrO_2 (*X* = 2, 3, 4, and 5) catalysts decreased with increasing H_2O/P123 mass ratio (*X*). It should be noted that composition of C_2 compounds such as C_2H_4 and CH_3CHO over Ni/2-ZrO_2 catalyst was much higher than that over Ni/5-ZrO_2 catalyst. The above results indicate that C–C bond cleavage reaction ($CH_3CHO + H_2O + O_2 = 2CO_2 + 3H_2$, $C_2H_4 + 2H_2O = CO_2 + CH_4 + 2H_2$), water–gas shift reaction ($CO + H_2O = CO_2 + H_2$), and methane steam reforming reaction ($CH_4 + H_2O = CO + 3H_2$) were accelerated with developing tetragonal phase of zirconia in the Ni/*X*-ZrO_2 (*X* = 2, 3, 4, and 5) catalysts. This is well consistent with the fact that tetragonal phase of zirconia was more efficient than monoclinic phase of zirconia for improving the catalytic performance of supported Ni catalysts [31].

4. Conclusions

X-ZrO_2 (*X* = 2, 3, 4, and 5) supports were successfully prepared by a sol–gel method with a variation of H_2O/P123 mass ratio (*X*). Ni catalysts supported on *X*-ZrO_2 (*X* = 2, 3, 4, and 5) were then prepared by an incipient wetness impregnation method for use in hydrogen production by auto-thermal reforming of ethanol. The effect of H_2O/P123 mass ratio (*X*) on the catalytic performance of Ni/*X*-ZrO_2 (*X* = 2, 3, 4, and 5) catalysts was investigated. Crystal structure and physical property of zirconia could be controlled by changing the H_2O/P123 mass ratio (*X*). With increasing H_2O/P123 mass ratio, surface morphology of zirconia was changed from rod-like shape to vesicle-like shape, and crystal structure was transformed from monoclinic phase into tetragonal phase. Crystal structure of zirconia strongly affected the catalytic performance of supported Ni catalysts in the auto-thermal reforming of ethanol. The catalytic performance increased in order of Ni/2-ZrO_2 < Ni/3-ZrO_2 < Ni/4-ZrO_2 < Ni/5-ZrO_2. Hydrogen selectivity over Ni/*X*-ZrO_2 (*X* = 2, 3, 4, and 5) catalysts was monotonically increased with decreasing reduction peak temperature (with increasing reducibility) and with increasing H_2O/P123 mass ratio. Although high catalytic performance of Ni/5-ZrO_2 was mainly due to the high reducibility of nickel species caused by the formation of pure tetragonal phase zirconia, it is believed that high surface area and small nickel crystalline size of Ni/5-ZrO_2 were also responsible for high catalytic performance of Ni/5-ZrO_2 catalyst.

Acknowledgements

The authors would like to acknowledge funding from the Korea Ministry of Knowledge Economy (MKE) through "Energy Technology Innovation Program".

References

[1] M. Schrope, Nature 414 (2001) 682.
[2] A. Haryanto, S. Fernando, N. Murali, S. Adhikari, Energy Fuels 19 (2005) 2098.
[3] S.D. Badmaev, P.V. Snytnikov, Int. J. Hydrogen Energy 33 (2008) 3026.
[4] A. Denis, W. Grzegorczyk, W. Gac, A. Machocki, Catal. Today 137 (2008) 453.
[5] J. Sun, D. Luo, P. Xiao, L. Jigang, S. Yu, J. Power Sources 184 (2008) 385.
[6] J.G. Seo, M.H. Youn, K.M. Cho, S. Park, S.H. Lee, J. Lee, I.K. Song, Korean J. Chem. Eng. 25 (2008) 41.
[7] M.H. Kim, E.K. Lee, J.H. Jun, C.Y. Han, S.J. Kong, B.K. Lee, T.J. Lee, L.J. Yoon, Korean J. Chem. Eng. 20 (2003) 835.
[8] D.J. Moon, J.W. Ryu, S.D. Lee, B.S. Ahn, Korean J. Chem. Eng. 19 (2002) 921.
[9] Y. Liu, T. Hayakawa, T. Tsunoda, K. Suzuki, S. Hamakawa, K. Murata, R. Shiozaki, T. Ishii, M. Kumagai, Top. Catal. 22 (2003) 205.
[10] S. Cavallaro, V. Chiodo, A. Vita, S. Freni, J. Power Sources 123 (2003) 10.
[11] B.M. Güell, I. Babich, K. Seshan, L. Lefferts, J. Catal. 257 (2008) 229.
[12] F. Romero-Sarria, J.C. Vargas, A.-C. Roger, A. Kiennemann, Catal. Today 133 (2008) 149.
[13] H. Wang, J.L. Ye, Y. Liu, Y.D. Li, Y.N. Qin, Catal. Today 129 (2007) 305.

[14] A.J. Akande, R.O. Idem, A.K. Dalai, Appl. Catal. A 287 (2005) 159.
[15] H.V. Fajardo, L.F.D. Probst, Appl. Catal. A 306 (2006) 134.
[16] X. Li, J.-S. Chang, S.-E. Park, React. Kinet. Catal. Lett. 67 (1999) 375.
[17] K.V.R. Chary, K. Ramesh, D. Naresh, P.V.R. Rao, A.R. Rao, V.V. Rao, Catal. Today 141 (2009) 187.
[18] M.H. Youn, J.G. Seo, K.M. Cho, J.C. Jung, H. Kim, K.W. La, D.R. Park, S. Park, S.H. Lee, I.K. Song, Korean J. Chem. Eng. 25 (2008) 236.
[19] G. Zhou, Y. Chen, J. Yang, S. Yang, J. Mater. Chem. 17 (2007) 2839.
[20] L. Calvillo, V. Celorrio, R. Moliner, P.L. Cabot, I. Esparbé, M.J. Lázaro, Micropor. Mesopor. Mater 116 (2008) 292.
[21] M. Selvaraj, S. Kawi, J. Mater. Chem. 17 (2007) 3610.
[22] R. Bandula, M. Vasilescu, H. Lemmetyinen, J. Colloid Interf. Sci. 287 (2005) 671.
[23] P. Biswas, D. Kunzru, Int. J. Hydrogen Energy 32 (2007) 969.
[24] M. Yamasaki, H. Habazaki, K. Asami, K. Izumiya, K. Hashimoto, Catal. Commun. 7 (2006) 24.
[25] C.A. Luengo, G. Ciampi, M.O. Cencig, C. Steckelberg, M.A. Laborde, Int. J. Hydrogen Energy 17 (1992) 677.
[26] Y. Yang, J. Ma, F. Wu, Int. J. Hydrogen Energy 31 (2006) 877.
[27] A.N. Fatsikostas, X.E. Verykios, J. Catal. 225 (2004) 439.
[28] Y. Matsumura, T. Nakamori, Appl. Catal. A 258 (2004) 107.
[29] R. Takahashi, S. Sato, T. Sodesawa, M. Yoshida, S. Tomiyama, Appl. Catal. A 273 (2004) 211.
[30] J.G. Seo, M.H. Youn, I.K. Song, J. Power Sources 168 (2007) 251.
[31] M. Benito, R. Padilla, L. Rodríguez, J.L. Sanz, L. Daza, J. Power Sources 169 (2007) 167.